Full length article

A method for the assessment and compensation of positioning errors in industrial robots

Sergio Ferrarini [a], Pietro Bilancia [a,*], Roberto Raffaeli [a], Margherita Peruzzini [b], Marcello Pellicciari [a]

[a] Department of Sciences and Methods for Engineering, University of Modena and Reggio Emilia, Reggio Emilia, Italy
[b] Department of Engineering Enzo Ferrari, University of Modena and Reggio Emilia, Modena, Italy

ARTICLE INFO

ABSTRACT

Industrial Robots (IR) are currently employed in several production areas as they enable flexible automation and high productivity on a wide range of operations. The IR low positioning performance, however, has limited their use in high precision applications, namely where positioning errors assume importance for the process and directly affect the quality of the final products. Common approaches to increase the IR accuracy rely on empirical relations which are valid for a single IR model. Also, existing works show no uniformity regarding the experimental procedures followed during the IR performance assessment and identification phases. With the aim to overcome these restrictions and further extend the IR usability, this paper presents a general method for the evaluation of IR pose and path accuracy, primarily focusing on instrumentation and testing procedures. After a detailed description of the experimental campaign carried out on a KUKA KR210 R2700 Prime robot under different operating conditions (speed, payload and temperature state), a novel online compensation approach is presented and validated. The position corrections are processed with an industrial PC by means of a purposely developed application which receives as input the position feedback from a laser tracker. Experiments conducted on straight paths confirmed the validity of the proposed approach, which allows remarkable reductions (in the order of 90%) of the orthogonal deviations and in-line errors during the robot movements.

1. Introduction

Nowadays, Industrial Robots (IR) are assuming a primary role in the modern factories owing to their extended operational flexibility, high operation speed and ability to handle and process a wide range of products. However, the application of IR in precision engineering fields still faces limitations, particularly when position accuracy becomes a critical aspect for the process, as in the case of additive or subtracting manufacturing operations. By leveraging their relatively good unidirectional pose repeatability (typically in the order of 50 to 100 μm), robots are currently employed in operations like picking and placing, assembly, welding, painting, and packaging, namely for repetitive tasks in structured environments [1]. In such applications, the use of manually imposed teaching points on the robot's end-effector path, together with the absence of external critical loads, allow to meet the requirements in terms of operational accuracy and product quality. On the other hand, the poor multi-directional repeatability (rarely specified in robot's datasheets and usually worse than the unidirectional repeatability) and volumetric accuracy (typically over

1 mm, as reported in Refs. [1–3]) of IR justify the rather limited use in precise machining operations, which are still mostly performed with special purpose devices [4,5]. In fact, compared to dedicated industrial equipment (e.g. numerical controlled machine tools), the IR open kinematic chain suffers of low structural stiffness and backlash-like nonlinearities which inevitably affect the overall position accuracy at the robot's end-effector [6,7].

With the aim to extend the IR operability and allow robot-based manufacturing processes, much research effort has been recently placed on IR performance characterization and improvement [8–12]. To quantify the robot accuracy experimentally, one may resort to different measuring instruments. In particular, optical and infrared systems can be considered due to their fairly low purchase price and the possibility to track up to 6 Degrees Of Freedom (DOF). Nevertheless, depending on the selected model, their measurement accuracy typically ranges from 0.1 mm to few millimeters (i.e. in this case comparable to that of many IR models, as reported in Refs. [13,14]) which makes them unsuitable for high quality performance testing and identification. Conversely,

ballbars can reach an accuracy of 1 μm [15,16], although they only perform planar measurements with a rather limited range of motion. In this context, Laser Trackers (LT) offer a good compromise as they can measure 3 or 6 DOF (depending on the model) with a final accuracy ranging from 10 to 100 μm on a much larger workspace. LT technology is widely adopted in robotics also due to its easy installation and high frequency measuring capabilities, as documented in Refs. [5,17–20].

The assessment of robot position accuracy must follow the ISO 9283 standard [21] which, however, does not provide detailed information on the testing methods. Actually, the lack of uniformity in testing procedures has led previous research works to different results making it challenging to compare their findings. One problem arises from the need to refer all measurement data to the Robot Base Frame (RBF) since no guidelines on how to perform the coordinate transformations between the sensor frame and RBF are provided in the norm [22]. In relation to this point, researchers have followed different approaches over the years. For example, in Ref. [23] a classical method for defining Tool Center Point (TCP) position is used, that is not very accurate, resulting in estimated error up to 6 mm propagated through all subsequent measurements. Differently, the method reported in Ref. [17] allows to accurately locate the TCP. In that work, however, the length of certain links is taken from the datasheet instead of directly measured on the robot and thus uncertainty is introduced. An exhaustive discussion on the RBF identification can be found in Ref. [22], though the reported comparisons only refer to the repeatability of the methods and not to their accuracy. An efficient method for determining the RBF is named Circle Point Analysis (CPA), which is typically utilized for robot kinematic calibration (i.e. measuring real Denavit–Hartemberg parameters), as shown in Refs. [24–26]. From the literature review, other gaps also emerged regarding the IR position performance identification, i.e.: (i) tests are normally performed in a single operating condition; (ii) the effect of lubricant temperature is not properly assessed and described; (iii) data post-processing is usually not outlined causing inability of repeating experiments.

As for the IR accuracy improvement, many approaches have been proposed either based on offline or online compensations. The first type utilizes a model-based schematic where position corrections are evaluated from previous measurements [9,27–29]. Despite their inherent simplicity, these methods have shown many limitations, primarily related to the difficulty of elaborating multi-parameter explicit models of the robot error over large workspaces. Furthermore, one should consider that the experiments are valid for the single robot model and must be repeated for different operating conditions or state of degradation of the robot. For these reasons, online compensation methods are usually preferred due to their more general structure and superior performance [5,19,30–33]. Here the position corrections are computed via a purposely conceived sensor guided closed-loop algorithm which cyclically communicates with both sensor (e.g. LT) and IR controller. As the main drawbacks, the software integration of these devices may become cumbersome due to the real-time constraints and, during the commissioning phases, proper tuning operations (e.g. for control gains and filters) become necessary to stabilize the control action. Previous researches have already proposed and validated efficient compensation strategies, although the following points are still unsolved or need more discussion: (i) compensation is restricted to path orthogonal deviations and does not consider in-path errors (causing the robot speed to be unstable during the traveling); (ii) controller tuning operations are rarely outlined and (iii) there is limited mention of the fundamental parameters that influence the control system during online compensation.

With the aim to overcome the above-discussed limitations concerning IR positioning performance assessment, the present paper reports on advances in experimental methods and guidelines for data acquisition, processing and correlation. Additionally, it provides a more comprehensive understanding of the potential metrology-based control solutions aimed at improving the IR accuracy, by discussing the primary process parameters involved and identifying the current limitations in implementing these solutions on modern IR controllers. Specifically, the novel contributions of this work are as follows:

- To define and thoroughly explain an universal method to assess the IR position accuracy performance. The reported procedure is validated on high payload KUKA IR and all measurements are carried out with a FARO LT within a flexible robotic cell for manufacturing (installed at the university facilities).
- To present the results of the experimental accuracy campaign under different working conditions (end-effector speed, applied payload and temperature state of the robot) and discuss their influence on the robot absolute positioning and path accuracy.
- To develop and test a control solution aimed at reducing the IR total spatial path tracking error (i.e. vector sum of orthogonal deviation and in-line error).

Detailed descriptions of the employed experimental setup, also covering installation and configuration aspects, are given throughout the paper.

The rest of the paper is structured as follows: Section 2 describes the experimental setup; Section 3 outlines the method studied for quantifying the robot pose and path accuracy; Section 4 presents and discusses the results of the experiments carried out on the KUKA robot; Section 5 reports and validates a novel approach for path error compensation; Section 6 provides the concluding remarks.

2. Experimental setup

In this section, the test equipment utilized for the experiments is outlined, as well as the two cell configurations established to achieve different objectives, i.e. respectively to quantify IR accuracy and implement error compensation strategies. The described setup will be promptly recalled in Section 3 to support discussions on the experimental methods.

2.1. Equipment overview

The research activities are conducted in the context of a flexible manufacturing robotic cell installed at the University facility and, in particular, by considering the following equipment:

- A KUKA KR210 R2700 Prime IR having a total mass of 1111 kg, a maximum payload of 210 kg and a maximum reach of 2700 mm. The IR is controlled by a KRC4 controller, featuring the software KSS version 8.3.25.
- A LT (FARO Vantage E) metrology system, whose motorized head sends a laser beam to the Spherical Mounted Retroreflector (SMR) tool attached to the robot's end-effector and measures its spatial position (x, y, and z coordinates) in a timely manner with respect to the coordinate frame of the laser emission source. The LT is positioned on a tripod with vibrations damping effect.
- A Thermal camera (FLIR A310), here adopted for assessing joints/ links temperature and verifying the achievement of thermal stability. While this sensor does not give the temperature of the internal oil (as previously done in Ref. [34] with thermocouple probes), it effectively shows the overall working condition of the manipulator [35].
- An Industrial PC, i.e. a Beckhoff CX-5140 exploited to run the developed real-time path compensation algorithm and send position corrections to the robot controller at each cycle time.
- A Laptop PC (Dell 3530), mainly used as an offline programming environment and for the post-processing of the acquired data.

A conceptual schematic of the employed hardware and related connections is reported in Fig. 1. As a research cell focused on industrial applications, it is equipped with various manufacturing tools, such as a
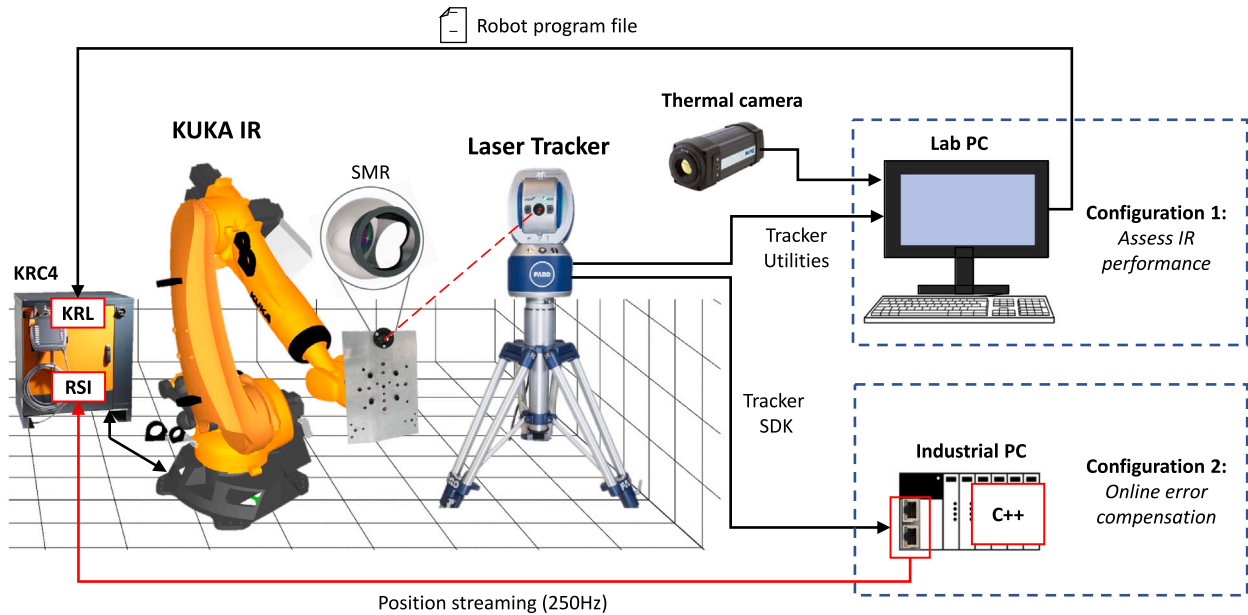
Fig. 1. Schematic of the employed setup and cell configurations. In the picture, KRL and RSI respectively indicate the KUKA Robot Language and the Robot Sensors Interface package for real-time external control.
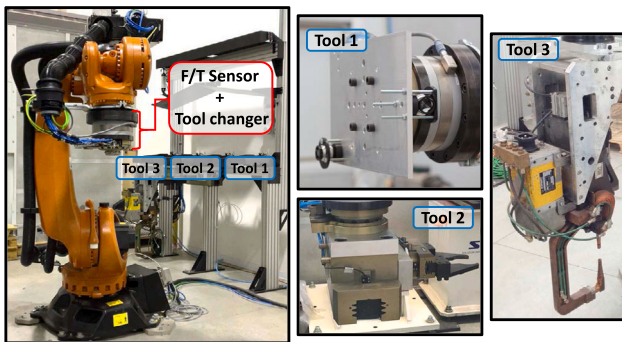

Fig. 2. Available tools for IR assessment: plate (tool 1), industrial gripper (tool 2) and spot welding gun (tool 3).

gripper and a spot-welding tool (see Fig. 2). These devices will be used as weight loads on the robot's end-effector during the accuracy assessment. To facilitate this, each of them has been disposed to securely hold the SMR during dynamic measurements. The SMR is placed on its magnetic base, which is attached to the metallic surface using both glue and screws.

2.2. Cell configurations

In the first cell configuration, namely the one established for the IR accuracy characterization, the KUKA robot is programmed with standard offline approaches. In practice, the KUKA Robot Language (KRL) code incorporating all the necessary linear (LIN command) and joint (PTP command) movement instructions is produced on the laptop PC (using WorkVisual environment) and then downloaded on the KRC4 computer, which is in charge of the entire robot control and supervision. During the tests, the LT measurements are managed through the FARO Tracker Utilities, which automatically retrieve information from the tracker control unit. Results are saved into text files containing the sampled data (acquired at a frequency of 1000 Hz) and related timestamp. In the first cell configuration, the absence of trigger signals

between IR and LT makes it necessary to use specific routines during post-processing to synchronize the start and end of the reading and thus compute errors. As for the thermal imaging camera, all the settings and acquisitions are made through the native camera monitor tool provided by FLIR.

For the purpose of developing an external path compensation module capable of being implemented on real industrial assets, the cell configuration must be modified. In particular, the robot motion profiles can no longer be generated from the KRC4 based on the provided KRL code, but are computed externally and applied through the KUKA Robot Sensor Interface (RSI) package. During RSI control, the KRC4 must receive a new position setpoint every 4 ms (i.e. input frequency of 250 Hz). Data exchange occurs by and from the KRC4 in XML format. Concerning the LT acquisition, there are no pre-compiled software allowing real-time data measurement and streaming. Therefore, a customized solution is developed in C++ by exploiting the FARO Software Development Kit (SDK). The signal synchronization is managed at code level by taking the RSI tic as the reference clock for the application. In practice, once a new RSI cycle starts, a request for a new position feedback is sent to the LT via the SDK libraries. As a response, the LT provides the last sample (and its time-stamp for precise input time shift calculation) to the controller. Unfortunately, the time required to get a measure from the LT suffers an unpredictable time delay (usually from 1 to 4 ms). After this delay, which does not impact the compensation algorithm as it always falls within the imposed RSI cycle time, the tracker will promptly provide all missing data. To prevent higher delays, a routine is included in the controller to handle situations with missed packages. The routine has a maximum number of allowed delayed packages before it stops the application and requests operator intervention.

The elaborated C++ program also contains the robot path generation and compensation functions as well as the communication with the KRC4. To maximize the control performance and reduce possible communication errors, the application is run on the Beckhoff industrial PC (Windows 10 environment), embedded with two real-time capable Ethernet ports.
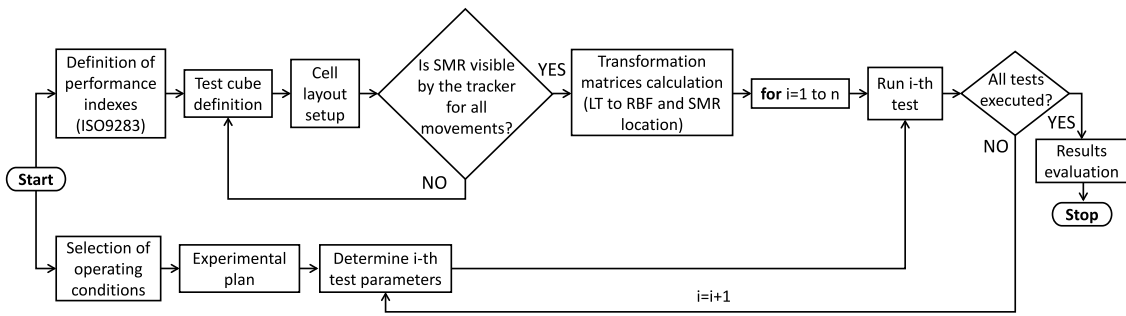
Fig. 3. Flowchart of the robot accuracy assessment.

2.3. Tracker measurements

As a fundamental step to perform valid experiments, the LT measurement capabilities must be first checked within the current experimental setup. At first, since the adopted LT can perform 3 DOF measurements (i.e. tracing of target position along X, Y and Z axes), the robot's end-effector orientation (A, B and C in KUKA) is not detected and, therefore, the tool is assumed to have a constant orientation during the experiment. For a complete assessment, one could adopt a LT enabling 6 DOF tracking (e.g. the FARO Vantages[6] or the Leica AT402) or, alternatively, install additional SMR on the end-effector, although in the latter case some practical issues arise. At first, installing multiple SMRs on different planes may not be feasible for all end-effectors. Secondly, this method is not suitable for evaluating path accuracy as the LT must move from one SMR to the next for each point, collecting all required information and determining tool orientation during post-processing. This multi-step measuring process also makes it difficult to implement closed loop approaches with real-time constraints.

Usually, ISO 10360-10 is used to assess the tracker performance, but also ASME B 89.4.19 standard is quite common. LT measurements are strongly affected by external factors, such as airflow, environment temperature, vibrations and floor deformation [36]. On the FARO manual, the LT accuracy is specified to be 20 μm + 5 μm/m (i.e. it deteriorates of additional 5 μm for every meter of distance between the LT and the SMR), while no repeatability values are provided. Regardless of the considered acceptability threshold, the spatial interval in which the real point can be, starting from the measured point, has an ellipsoidal shape. Since the ellipsoid is squashed in the outgoing direction from the tracker, there is an anisotropy in the perception of the space surrounding the tracker (see [37] for more details). These considerations are the basis for the correct positioning/orientation of the instrument to obtain the best performance, as it will be shown in Section 3.

Concerning the LT repeatability, a test has been conducted inside the cell by placing a SMR target on a tripod and recording its static position for 1 h. During this period, environmental conditions were controlled (doors closed, minimal operators movements). As expected, the processed data reported a maximum peak to peak deviation sensibly lower in the direction aligned with the laser beam (0.02 mm against 0.3 mm). The LT repeatability in the environment is found to be around 54 μm. This value is similar to that of the employed IR (i.e. 60 μm, as declared in the robot datasheet), confirming the LT cannot be used for estimating the robot position repeatability. On the basis of these considerations and of the adopted setup, the present work focuses on the IR accuracy evaluation.

3. Accuracy assessment method

This section reports on experimental methods and procedures for the assessment of the IR positioning accuracy which are generally valid for any combination of anthropomorphic robot and metrology system. The proposed framework, validated on the industrial asset described in Section 2, can be summarized in the following basic steps:
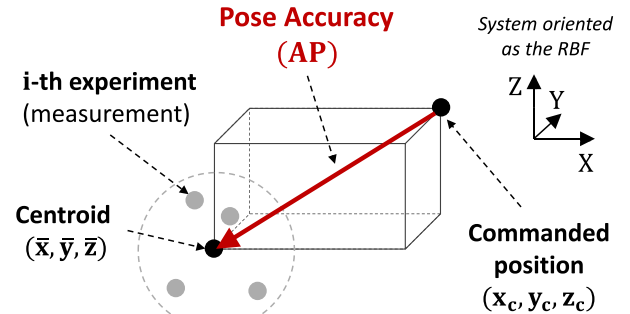

Fig. 4. Position accuracy principle (from ISO 9283).

1. Definition of performance indexes, based on ISO 9283;
2. Cell layout setup (LT positioning with respect to the IR's test working area);
3. Estimation of the coordinates transformation matrix (correlation between LT and IR frames);
4. Definition of experimental procedures and tested operating conditions.

A flowchart of the process is reported in Fig. 3. These aspects will be discussed in detail in the remaining of this section.

3.1. Performance indexes

In many industrial practices the pose repeatability is considered the only index worthy of expressing the error of the robot, so much that on many IR datasheets only this characteristic is reported. However, this statement is valid only when considering repetitive tasks, for which the robot has previously followed a manual teaching procedure. The emergent need for reconfigurable and autonomous robotic systems that can adapt to multiple tasks on extended workspaces, has moved the attention also to the pose accuracy. According to the ISO 9283, "Pose accuracy expresses the deviation between a command pose and the mean of the attained poses when approaching the command pose from the same direction". The following relation is given on the standard to quantify pose accuracy (AP):

$$AP = \sqrt{(x_c - \bar{x})^2 + (y_c - \bar{y})^2 + (z_c - \bar{z})^2} \qquad (1)$$

where x_c, y_c, z_c represent the spatial commanded position in the RBF and $\bar{x}$, $\bar{y}$, $\bar{z}$ are simply calculated for n repetitions as:

$$\bar{x} = \frac{1}{n}\sum_{i=1}^{n} x_i \quad \bar{y} = \frac{1}{n}\sum_{i=1}^{n} y_i \quad \bar{z} = \frac{1}{n}\sum_{i=1}^{n} z_i \qquad (2)$$

being x_i, y_i, z_i the reached position in the ith experiment expressed in the RBF. Fig. 4 represents graphically what expressed in previous formulas. Once correctly evaluated, AP assumes particular significance during offline programming as it allows to finely adjust the targets'
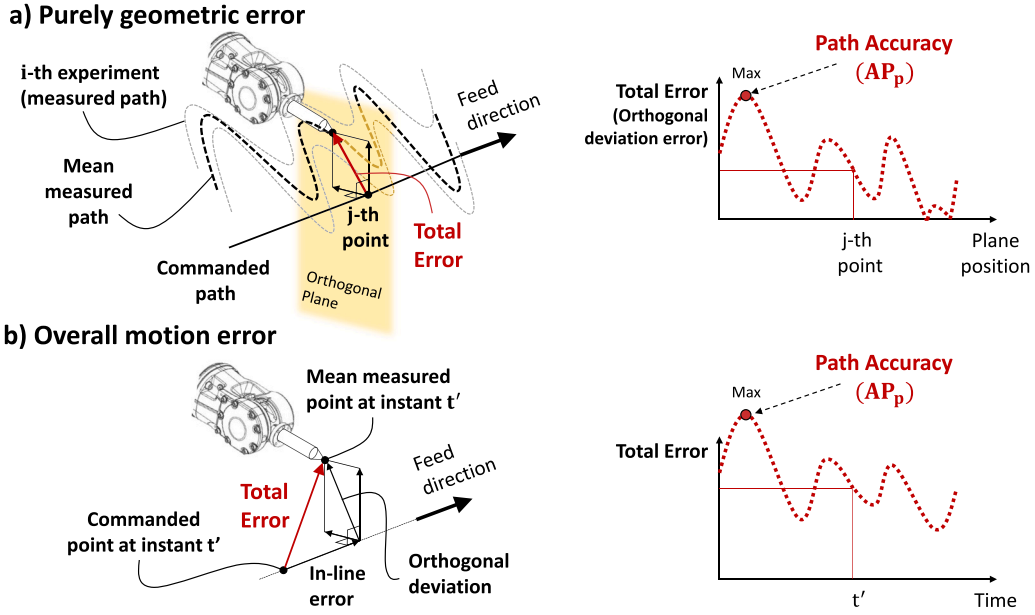
Fig. 5. Path characteristics and error calculation principle: (a) Offline experiments (b) Online experiments with time synchronization.

position. However, it does not account for errors made along the robot paths.

These are captured with dedicated experiments where the entire robot path is recorded as a series of m discrete points for n repetitions. The path accuracy index (AT_p) is then calculated in the RBF as follows:

$$AT_p = max\left(\sqrt{(x_{c,j} - \bar{x}_j)^2 + (y_{c,j} - \bar{y}_j)^2 \atop +(z_{c,j} - \bar{z}_j)^2}, \quad j = 1, \dots, m\right) \quad (3)$$

where $\bar{x}_j$, $\bar{y}_j$ and $\bar{z}_j$ are the mean values of the n measurements performed for the jth point, i.e.:

$$\bar{x}_j = \frac{1}{n}\sum_{i=1}^{n} x_{j,i} \quad \bar{y}_j = \frac{1}{n}\sum_{i=1}^{n} y_{j,i} \quad \bar{z}_j = \frac{1}{n}\sum_{i=1}^{n} z_{j,i} \quad (4)$$

For a given path, AT_p reveals the maximum deviation of the obtained mean path from the ideal (i.e. commanded) one. As shown in Fig. 5, the error can be calculated in two ways depending on whether the commanded path only includes geometric information (i.e. when the IR is moved with standard instructions and time synchronization between LT and robot is not guaranteed, as in the first cell configuration of Fig. 1) or if it is a real-time controlled series of points (as in the second cell configuration). In the former setup (aimed at characterization), errors are calculated orthogonal to the commanded path, whereas in the latter setup (aimed at compensation) an error parallel to the path (called in-line error) can also be identified, contributing to the overall error. The in-line error can be further split into geometric error, due to the mechanical system, and control error, which can be seen as the end-effector's anticipation/delay with respect to the planned in-line position at a certain time. Naturally, to calculate the orthogonal deviation for paths executed along the RBF principal axes, only two of the three directional errors listed in Eq. (3) are considered.

3.2. Installation practices

The ISO 9283 specifies that tests have to be performed inside a cube, which is defined based on the following criteria: (i) it shall be located in the portion of the IR workspace where the robot will be most frequently (or for a specific task) used; (ii) it shall have the largest possible volume while keeping its edges aligned with the RBF. Therefore, the primary definition of the measurement cube is based on the workspace
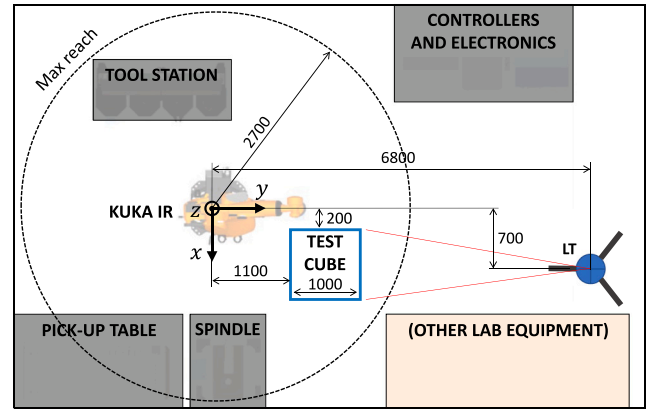

Fig. 6. Cell layout for experiments.

representation provided on the IR datasheet. Then, one must also check the extension and spatial configuration during functioning of the mounted tools (see Fig. 2) as well as the presence of possible obstacles (i.e. other cell devices) within the working environment. In the present case, the experiments are conducted within a flexible robotic cell for manufacturing and the measuring cube is located by considering the robot workspace close to the spindle to retrieve information that will be used during machining operations for improving part quality.

3D simulation software (e.g. KUKA.Sim or RoboDK) could facilitate this task and help in preventing from collisions during the testing. They also allow to check the robot configurations and avoid possible kinematic singularities, which would otherwise cause the robot to decelerate and even stop during the path execution. Actually, to properly assess the influence of the robot traveling speed on the path accuracy, it is essential to maintain a constant speed during each single experiment.

Once the previous conditions are met, the measuring cube's size and position must be further revised on the basis of the adopted instrumentation. In the specific case of a LT, the working distance between the tracker's head and the SMR must fall within a specific interval. In particular, a minimum distance is necessary for allowing the laser beam to reach the SMR at each programmed position in the cube (for all the mounted tools). On the other hand, increasing this distance
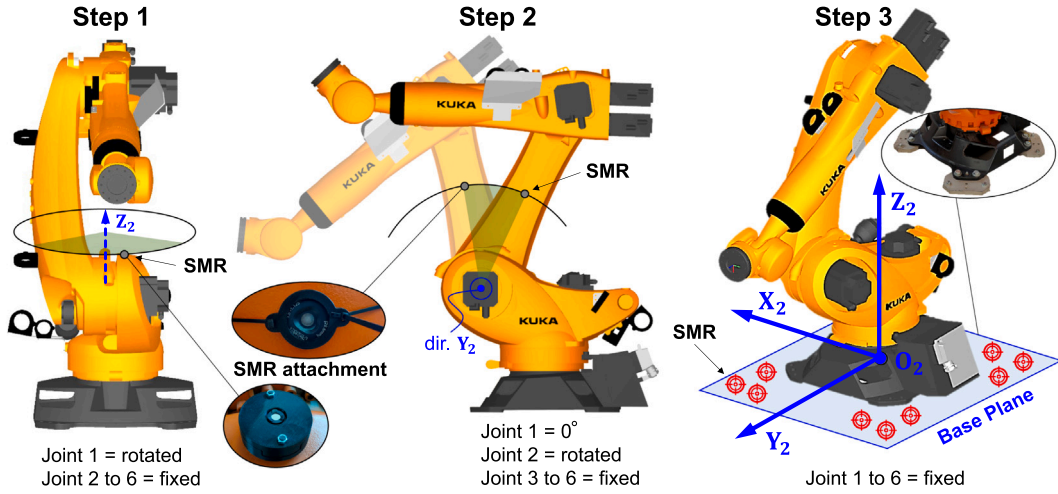
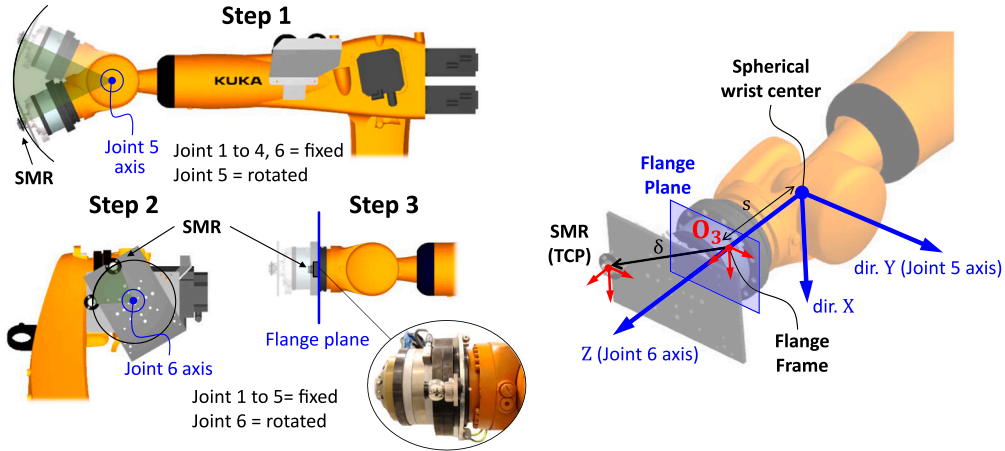**Fig. 7.** RBF evaluation through axes rotation and CPA.

Fig. 8. Determination of SMR position with respect to the robot flange frame through axes rotation and CPA.

will lower the LT measuring accuracy, as highlighted in Section 2.3. To visualize these concepts, a schematic of the cell layout adopted in this work is reported in Fig. 6. In the shown configuration, the cube's size is 1000 mm and the LT is installed at a distance of 5200 mm (i.e. $6800 - 1100 - 1000/2$) with respect to the cube's center point. This arrangement results in a measuring accuracy of approximately 46 µm (i.e. $20 + 5 \cdot 5.2$), using the formula reported in Section 2.3.

3.3. Frames identification

The position of a point measured with the LT is expressed in its own frame, while the robot pose is defined in the RBF. Hence, for accuracy estimation (i.e. error calculation), the following preliminary requirements are mandatory:

1. The transformation matrix to convert the LT sampled points in the RBF must be determined (once the cell layout is chosen [38]).
2. For each tool installed on the robot (see Fig. 2), the TCP must coincide with the SMR. In other words, the SMR offset with respect to the robot flange frame is to be measured and then specified in the controller settings as it will be used for the trajectory generation.

Both these steps are conducted experimentally adopting the CPA method, and the associated geometric relations are calculated during

post-processing. In particular, the CPA is based on moving the robot's joints one at a time and measuring the circular path described by a point where the SMR is fixed. In this way, kinematic and control errors are reduced to the extent possible since only single joint movements are commanded. Random errors, however, can be introduced by the LT, whose influence can be reduced with a large number of samplings. From the measured data, one could find the circle that best fits the path and thus derive the related joint's origin and axis of rotation [20].

1. Transformation matrix: with reference to Fig. 7, by assuming $O_1 X_1 Y_1 Z_1$ and $O_2 X_2 Y_2 Z_2$ respectively the LT frame and the RBF, the matrix can be written as:

$$\mathbf{T} = \begin{bmatrix} \mathbf{R_{3x3}} & \mathbf{t_{3x1}} \\ \mathbf{0_{1x3}} & 1 \end{bmatrix} \tag{5}$$

where $\mathbf{R_{3x3}}$ and $\mathbf{t_{3x1}}$ are the rotation matrix and the distance vector between the systems, i.e.:

$$\mathbf{R_{3x3}} = \begin{bmatrix} u_{x2} & v_{x2} & w_{x2} \\ u_{y2} & v_{y2} & w_{y2} \\ u_{z2} & v_{z2} & w_{z2} \end{bmatrix} \tag{6}$$

$$\mathbf{t_{3x1}} = \mathbf{R_{3x3}}(O_2 - O_1) \tag{7}$$

being u_2, v_2 and w_2 the components of versors of the RBF axes in the LT frame. The matrix $\mathbf{T}$ is defined such that its product with a vector representing the SMR spatial position in the LT frame will return the same vector in the RBF. The CPA-based procedure for its experimental identification is shown in Fig. 7 and involves the following steps:

- A rotation of joint-1 is performed to find the direction of the RBF's Z-axis (u_{z2}, v_{z2}, w_{z2}). To exclude any source of errors during the measurement (e.g. unwanted movements of the robot structure due to reducers backlash and compliance), the SMR is attached to the link closest to the joint in motion (i.e. link 1).

- After setting the joint-1 to its zero position, joint-2 is rotated to obtain the Y-axis (u_{y2}, v_{y2}, w_{y2}). At this step, the SMR is fixed to link 2. As the zero position of joint-1 can be reached with either clockwise or counterclockwise rotations, which may lead to slightly different results, the experiment is conducted under both conditions and the outputs are then averaged during post-processing.

- The X-axis (u_{x2}, v_{x2}, w_{x2}) is determined by taking the cross product of the Y-axis and Z-axis. To address the issue of non-orthogonality between the axes, the method outlined in Ref. [17] can be employed, which enforces orthogonality through a final vector product.

- A set of 9 points is measured by placing the SMR on the upper surface of the visible (i.e. LT accessible) robot's base supports to identify the base plane. Although only 3 points are theoretically needed for the calculation, each support exhibits irregularities and different inclinations due to production and installation errors, thus multiple measurements are taken.

- The origin O_2 is found by intersecting the base plane with the Z-axis.

The procedure must be repeated whenever the LT (or, eventually, the robot) location is varied inside the cell.

2. SMR position: For each mounted tool the SMR is fixed at a specific user-defined point, which should become the new TCP. In the robot control system, the TCP origin is specified with respect to the flange frame. Such distance can be obtained from CAD models, although using the CPA can yield more accurate results. In the latter case, similarly to the previous approach and according to Fig. 8, the transformation matrix between $O_1 X_1 Y_1 Z_1$ and $O_3 X_3 Y_3 Z_3$ is found as follows:

- An initial configuration with the last three robot joints set to zero is commanded.
- The SMR position in registered in static conditions.
- A rotation of joint-5 is imposed to find the Y-axis of the flange frame.
- Joint-5 is homed at zero and joint-6 is rotated to find the Z-axis.
- After installing another SMR on the flange plane, joint-6 is rotated again to identify such plane.
- The X-axis is obtained from the cross product. As discussed before, an additional product may be necessary to ensure perfect orthogonality. The center of the spherical wrist is identified from the intersection of the previous axes.
- The origin of the flange frame (O_3) is found by intersecting the flange plane with the Z-axis (i.e. at a distance s along the z coordinate from the wrist center).

Once $O_3 X_3 Y_3 Z_3$ is identified, the vector δ can be easily determined and the tool data updated during robot programming. To facilitate the implementation of the reported procedures, a sample of Matlab code addressing the data post-processing is included in the supplementary materials section.

3.4. Experimental procedure

All the experiments are performed with the following settings on the KRC4 controller:

1. *Absolute Accuracy* mode deactivated. This feature, provided by KUKA, is meant to improve accuracy of the robot, although it is typically provided upon extra costs and thus may not be available in every industrial cell. To suppress it, the value of the $DEACTIVATE_ABS_ACCUR system variable inside the custom.dat file is changed.

2. Correct the RBF orientation ($ROBROOT in KUKA) to allow the robot controller to correctly consider the gravity direction (Z-axis alignment based on the robot installation). Gravity-alignment can be made with the LT. This operation is performed at software level by editing the machine configuration.

3. Execute Mastering for each tool. Detailed procedures for this operation can be found on the robot manuals. The objective is to find the zero-point of all the axes at the output stage of gear reducers, which is slightly different for each type of load to be handled.

After completing these initial steps, the accuracy testing is carried out using the metrics specified in Section 3.1.

The pose accuracy is measured for five positions (repeated 30 times) within the designated measurement cube. The selected points lie on a plane formed by cutting the cube diagonally, as illustrated in Fig. 9. The points are located inside the cube (i.e. no intersection with the cube's faces). For each operating condition (described in Section 3.5) a single recording is generated. The robot is moved with a point-to-point motion (PTP instruction in KUKA) and a dwell time of 4 s is imposed at each point to allow system stabilization and measurement, which can be identified during post-processing by analyzing the acceleration plots. A threshold is then used to detect the samplings, and the final pose is obtained from their average value. After coordinate transformation from LT frame to RBF (matrix **T** in Eq. (5)) and direct comparison with the ideal (commanded) pose, the position accuracy is calculated as in Eq. (1).

For path accuracy tests, a set of 25 linear movements (LIN instruction in KUKA) is executed for each Cartesian direction in the RBF. The lines are disposed in planes parallel to the faces of the cube, as visible in Fig. 9. All the linear paths has been verified within RoboDK environment to confirm that the robot does not pass through any singular position. The first 50 mm of each line is run at a low and constant speed for all tests (50 mm/s) to obtain comparable starting data. For each direction of motion (i.e. X, Y and Z axes), the lines are repeated 3 times within a single LT record. During post-processing, all the linear paths are segmented into discrete points by intersecting them with a series of parallel planes. For each generated point, the determination of the orthogonal deviation error follows Eqs. (3) and (5). It should be once again recalled that in the current setup the in-line error has not been considered.

3.5. Parametric study

A parametric study has been carried out aimed at evaluating the robot accuracy for different operating conditions. The collected results will be organized to produce performance maps over the explored multi-domain, which comprises the following variables:

- *Workspace*: different points/lines are evaluated within the prescribed cube, each of them characterized by a specific number (as in Fig. 9). Note that cube dimensions and position are now considered fixed parameters.
- *Direction of motion*: path accuracy tests are executed along X, Y and Z axes (see Fig. 9).
- *Movement speed*: this is imposed as a percentage of the maximum allowed speed for PTP instructions and as a linear speed (mm/s) for LIN instructions. Since high joint speeds may be needed when traveling close to singularities, to ensure stable conditions and avoid controller issues, the maximum considered linear speed is set to 300 mm/s.
- *Payload*: corresponding to the 3 robot tools reported in Fig. 2, having a total mass of 30 kg (tool 1), 80 kg (tool 2) and 160 kg (tool 3), i.e. respectively 14%, 38% and 76% of the robot rated payload.
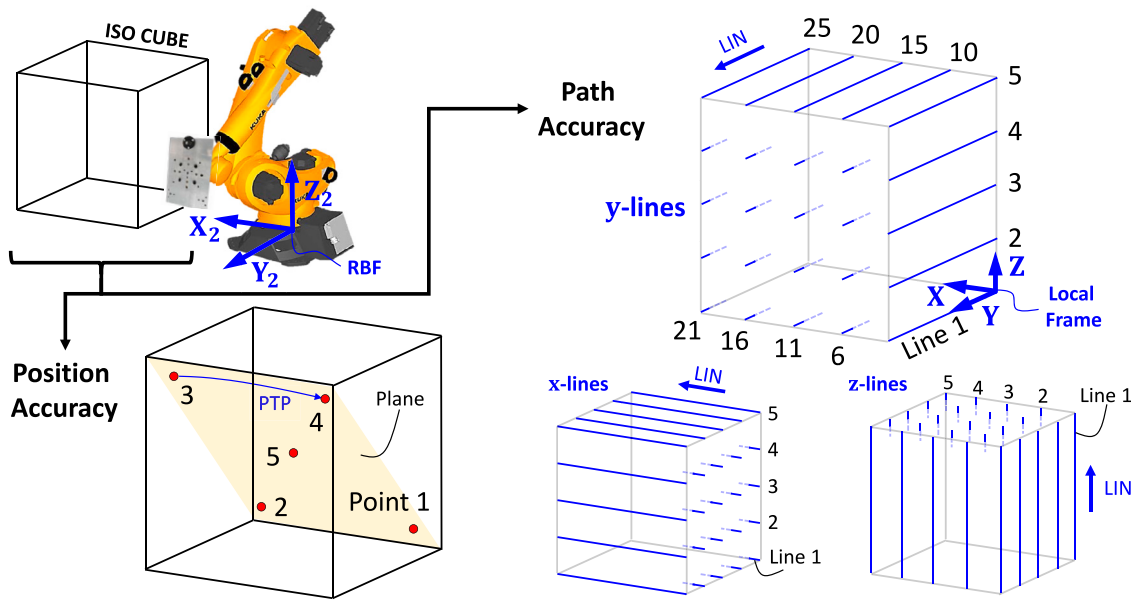
Fig. 9. Position and path test geometry: points and lines spatial distribution within the cubic workspace.
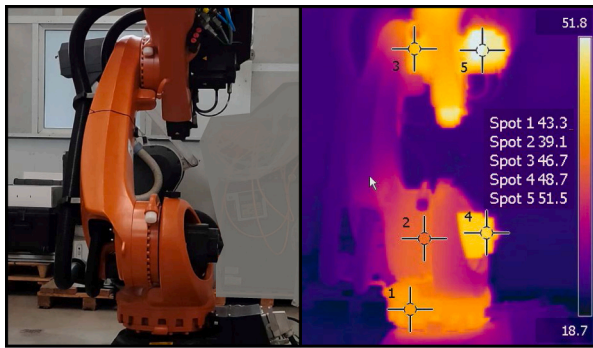

Fig. 10. Robot warmed up condition registered with the thermal camera after 2 h of cycling (temperature reported in °C).

Table 1
Parameters and values considered during the accuracy assessment on the KUKA robot.

Variable	Values	Unit
Pose accuracy		
Pose number	1, 2, 3, 4, 5	–
Speed	10, 50, 100	[%]
Payload	30, 80, 160	[kg]
Heating condition	Hot, cold	–
Path accuracy		
Line number	1 to 25	–
Direction of movement	x, y, z	–
Speed of motion	100, 200, 300	[mm/s]
Payload	30, 80, 160	[kg]
Heating condition	Hot, cold	–

- *Thermal state*: it refers to the temperature of the robot and of its servo modules. In this study, it has been distinguished in two cases: (i) Cold start (robot at environment temperature after several hours of inactivity) and (ii) Warmed-up (robot at steady-state temperature after running a cyclical program for a few hours).

While the effects of speed and payload have been deeply investigated in previous studies, the robot thermal condition has been rarely considered during accuracy assessments, although its influence on the dynamic behavior of IR and related servo modules can be seen in Refs. [34,39]. In this work, the effects of warming up the robot structure are monitored with the thermal camera. An example of heated condition, reached after 2 h of cycling, is reported in Fig. 10. It must be specified that precise information regarding the reducers' oil state are not available adopting an external sensor due to the high wall thickness of the robot components. Also, the temperature measured before starting the experiment (and after the warm-up phase) may fluctuate during operation depending on the applied speed and payload.

The experimental study has been structured as a grid comprising all the possible combinations between variables, whose values are summarized in Table 1. Overall, a total number of 90 points (repeated 30 times) and 1350 lines (repeated 3 times) are recorded.

4. Experimental results

This section presents the main outcomes of the experimental campaign carried out on the KUKA KR210 R2700 Prime robot. The collected results are hereafter reported and commented.

4.1. Pose accuracy

At first, the pose accuracy AP is evaluated in the RBF as in Eq. (1). A comparison of the results from the various conditions tested for points 1–5 is reported in Fig. 11. Statistical analyses have been conducted to highlight the dependency of AP from each parameter. Since normality hypothesis on the data distribution cannot be verified, non-parametric tests [40,41] are used to show the differences between operating conditions. In particular, two types of tests are considered:

- *Wilcoxon signed rank*: it is used to determine if there are significant differences in AP between pairs of data when a single parameter is varied (e.g. travel speed increased from 10% to 50%). The imposed null hypothesis is that the median difference between paired population is zero.
- *Friedman*: it is used to check if there is a dependency of AP on the target position in the robot's workspace (i.e. the measuring cube). In this case, the null hypothesis is that all the selected points have the same AP.
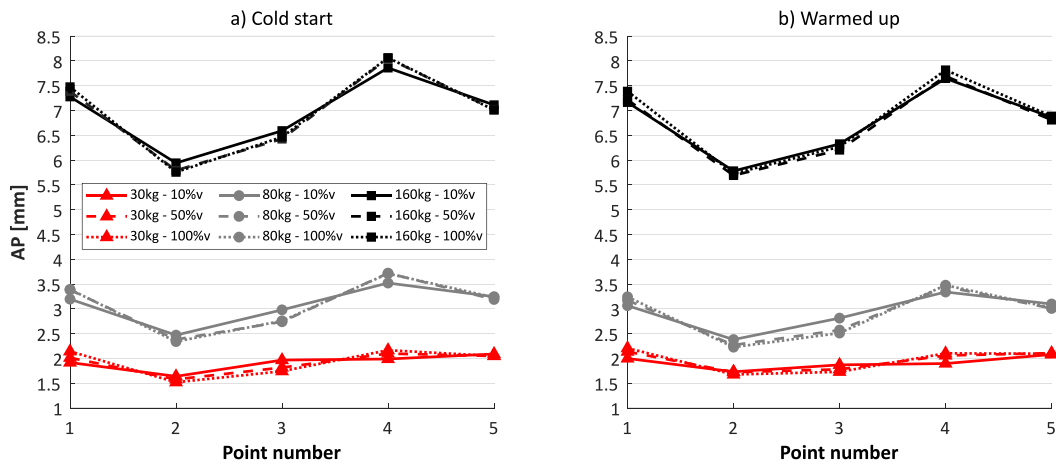
Fig. 11. Pose accuracy values of points 1 to 5 for all the tested conditions. Results have been divided in two plots, respectively for cold start (a) and warmed up (b) thermal states.

Table 2
Pose accuracy statistical results: effect of varying each single parameter on AP.

| Variation	Test type	p-value	Mean AP increment	Significance
Speed 10% to 50%	Wilcoxon	0.75	–	No
Speed 10% to 100%	Wilcoxon	0.57	–	No
Speed 50% to 100%	Wilcoxon	0.0822	–	No
Payload 30 kg to 80 kg	Wilcoxon	1.7e−6	1.06 mm	Yes
Payload 30 kg to 160 kg	Wilcoxon	1.7e−6	4.92 mm	Yes
Payload 80 kg to 160 kg	Wilcoxon	1.7e−6	3.86 mm	Yes
Hot to cold	Wilcoxon	5.5e−6	0.11 mm	Yes
Pose to pose	Friedman	1.3e−12	Up to 1.22 mm	Yes
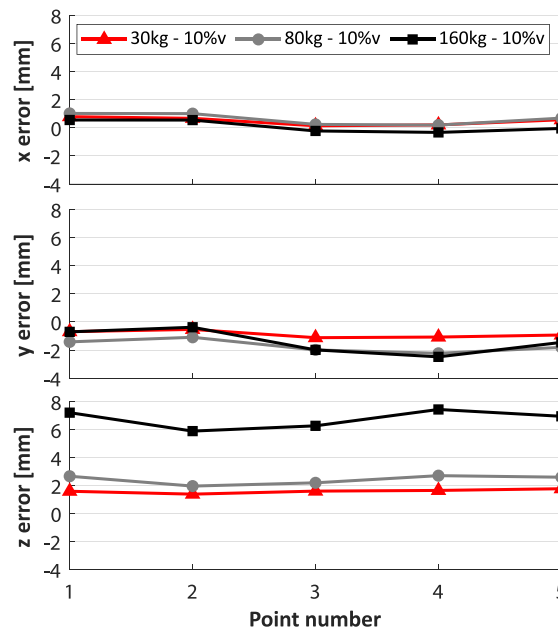
Fig. 12. Directional errors (calculated as $(x_c - \bar{x})$, $(y_c - \bar{y})$ and $(z_c - \bar{z})$, see Eq. (1)) for all samples.

To determine the significance of such hypotheses, the *p*-value has been calculated for each test (see Table 2). In particular, if the *p*-value is less than 0.05, the null hypothesis is rejected and a statistically significant difference between the conditions is found. In these cases, the mean AP increment is also calculated.

Overall, it can be observed that the payload has a great impact on the pose accuracy (AP variations up to 400% when stepping from tool 1 to tool 3, namely from 30 kg to 160 kg). As the payload increases, the error in the Z-axis becomes increasingly important, ultimately resulting in the dominant contribution of the overall position error, as shown in Fig. 12. Changing thermal state has good significance, as it can be noted from Fig. 11 and further confirmed in Table 2, although preheating the IR before operation only results in minimal accuracy improvements (in the order of few tenths). At last, it is found that the travel speed has
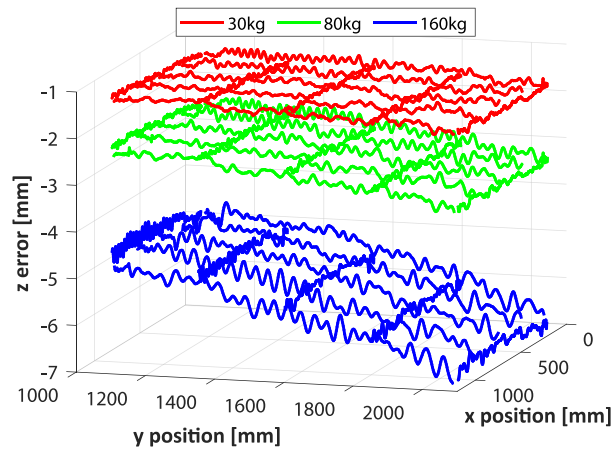
Fig. 13. Position error in z direction calculated in the RBF for *x* and *y* lines traveled at 100 mm/s (cold start).
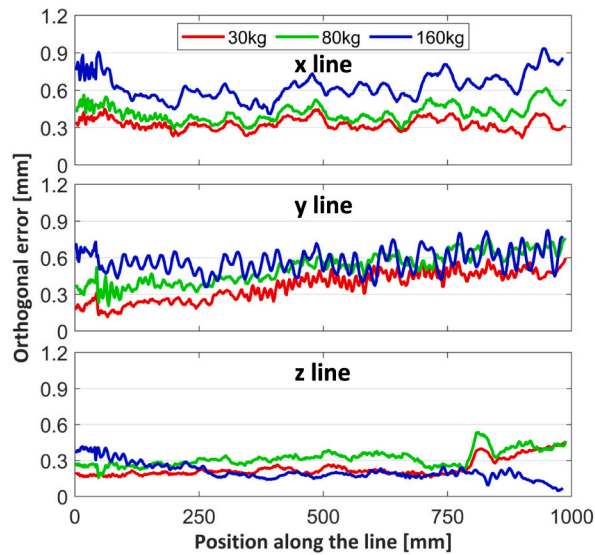

Fig. 14. Effect of payload on the orthogonal error along line 13, traveled for each direction at a speed of 100 mm/s (cold start).

little impact on AP, which is primarily influenced by the robot pose (see differences between points 2 and 4 in Fig. 11). For this reason, also depending on the specific robotic application, more poses may eventually be registered for a comprehensive volumetric analysis.

4.2. Path accuracy

Path results are analyzed referring to either the path accuracy index (AT_p) and the point-to-point orthogonal deviation error with respect to the ideal (commanded) lines. Such quantities have been initially computed in the RBF, as specified in the norm and reported in Section 3.1. However, the obtained AT_p values inevitably include AP, being the first point of a new line reached with a certain position error. This is clearly visible in Fig. 13, where the contribution of AP on the z error can be deduced for each plotted line after comparison with Figs. 11 and 12. Hence, to better identify the errors committed by the robot during path traveling, path results have been processed with respect to a local frame located at the corner of the cube where lines 1 of the x, y, and z directions intersect (Fig. 9).

Similarly to Section 4.1, a Wilcoxon signed rank statistical test is performed to investigate the AT_p dependency from each single parameter (payload, speed and thermal state). Then, two Friedman tests are conducted, respectively to check the influence of the line position

(i.e ranging from line 1 to 25) within the cube and of the travel direction (i.e. considering x, y, and z lines) on AT_p. From a close observation of the processed data, the following considerations can be made:

- An increasing payload leads to higher orthogonal errors, as visible in Fig. 14 and confirmed by the comparisons reported in Table 3. Error plots exhibit higher mean values and amplified oscillations, with a particularly pronounced effect on the *x* and *y* lines.
- Differently from pose accuracy, higher traveling speeds negatively impact the robot path accuracy, as it can be seen in Fig. 15 and in Table 3. In particular, the harmonic content plotted for each line shows an amplification of the main peaks. Overall, errors are in the frequency range between 0 and 15 Hz. A frequency shift is observed between the curves at different speeds which can be possibly attributed to joint mechanical transmission errors. Indeed, as discussed in Ref. [39], position dependent reducer errors, corresponding e.g. to eccentricity and tooth-to-tooth errors, manifest at specific positions in the angular domain (i.e. a certain number of times per each revolution of the output shaft), which means that their frequency in the time domain shifts in the spectrum based on the operated angular speed.

Table 3
Path accuracy statistical results: effect of varying each single parameter on AT_p.

| Variation	Test type	p-value	Mean AT_p increment	Significance
Speed 100 to 200 mm/s	Wilcoxon	2.7e−54	0.07 mm	Yes
Speed 100 to 300 mm/s	Wilcoxon	1.5e−61	0.11 mm	Yes
Speed 200 to 300 mm/s	Wilcoxon	4.22e−25	0.04 mm	Yes
Payload 30 kg to 80 kg	Wilcoxon	1.6e−73	0.18 mm	Yes
Payload 30 kg to 160 kg	Wilcoxon	6.7e−65	0.29 mm	Yes
Payload 80 kg to 160 kg	Wilcoxon	4.08e−24	0.11 mm	Yes
Cold to hot	Wilcoxon	3.6e−5	0.02 mm	Yes
Direction of motion	Friedman	3.1e−52	Up to 0.22 mm	Yes
Line to line	Friedman	7.1e−153	Up to 1.03 mm	Yes
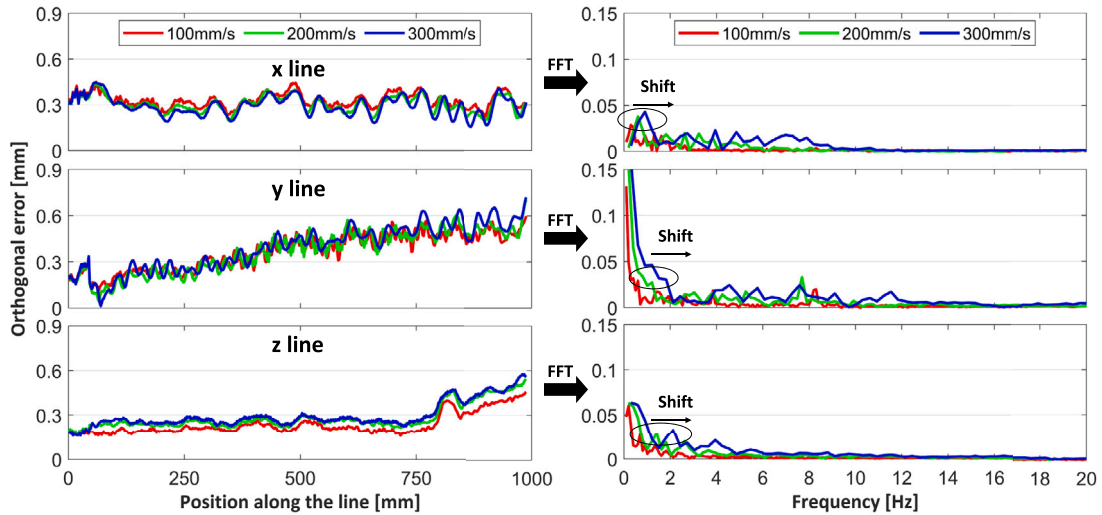
Fig. 15. Effect of speed on the orthogonal error along line 13, traveled for each direction with a payload of 30 kg (cold start). In the picture, FFT indicates the Fast Fourier Transform.
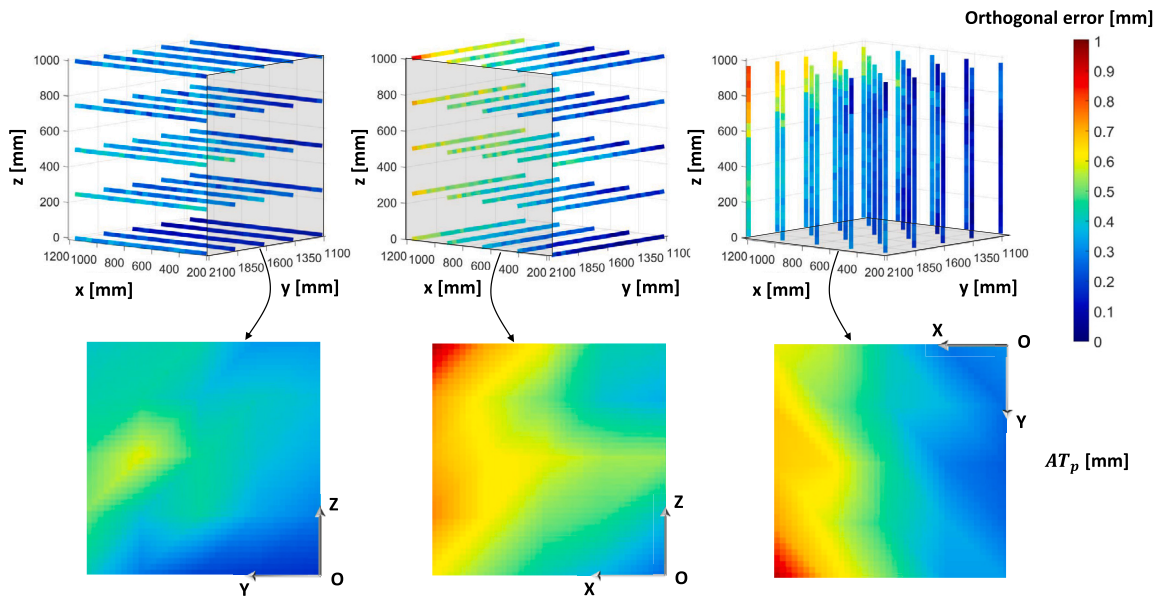

Fig. 16. Contour plot of orthogonal error and AT_p for lines traveled at 100 mm/s with a payload of 30 kg (cold start).

- The maximum path error (and AT_p value) has been registered for y lines, while z lines show the best performance, as visible in Fig. 16.
- Overall, great variability is registered between lines of the same direction (i.e. ranging from line 1 to 25), highlighting the strong dependence of the robot's dynamic behavior on its assumed configuration (as also confirmed by the results shown in Section 5).

- Warming up the robot leads to limited changes on the path error, being the mean AT_p increment equal to 0.02 mm. Such value is comparable with the LT accuracy.

The complete dataset of the performed experiments is shared from the supplementary material section, including scripts for results processing and visualization.

The conducted tests have successfully validated the methodology presented in Section 3. The approach, which turned out to be solid and straightforward, can be easily applied to any serial manipulator and designed path, allowing programmers and system integrators to establish correlations among parameters and position errors, and facilitating the deployment, calibration and predictive maintenance of existing cells, as well as the commissioning of new ones.

5. Path error online compensation

This section describes an online control strategy aimed at reducing the robot errors during path execution. As discussed in Section 1, most of the available offline compensation algorithms partially solve the accuracy errors of serial manipulators. This is mainly due to the complexity of defining precise compensation models given the high number of variables affecting the robot performance, namely: speed, payload, temperature, kinematic configuration and direction of motion (see differences in results for various pose/line numbers in Fig. 16), reducer type and state, and general state-of-degradation of the system. In the specific case of the tested KUKA robot, if the *Absolute Accuracy* mode is active (meaning $DEACTIVATE_ABS_ACCUR is set to FALSE), significant reductions in the position error are observed during pose reaching as a result of the payload weight compensation obtained with precise stiffness models of the manipulator. This is a favorable outcome as the payload is the primary contributor to pose accuracy errors, as visible in Fig. 13. However, during path execution, where servo reducer kinematic errors have significant impact on the end-effector motion, path deviations and in-line errors are still present. To solve for these, an online compensation appears to be the most appropriate solution since it can potentially detect and compensate for any error source that occur within the controller's bandwidth.

For this purpose, the previous setup has been modified to allow the implementation of an external trajectory compensation module, as illustrated in Section 2.2. To enable externally guided motion, the following configurations on the KRC4 controller have been established:

1. Sensor mode set to IPO_FAST so as to work with minimum cycle time (4 ms).
2. Correction type set to *Sensor-Guided Motion*. This excludes any internally generated motion profile to be executed and enables the external trajectory streaming.
3. Coordinate system for Cartesian corrections set to *Absolute*. This system has its origin in the first point of RSI activation and is oriented as the RBF.

The compensation module (running on the industrial PC, as shown in Fig. 1) is based on a closed loop algorithm subject to real-time constraints imposed by the RSI. In particular, recalling Section 2.2, once a new RSI cycle starts, a request for position feedback is sent to the LT which in turn provides the last sampled data to the compensation module. This performs error computation (involving coordinate transformation from LT frame to RBF), and provides path correction data to the RSI within the current cycle. The novelty of the proposed solution lies in the compensation of both orthogonal deviation and inline error (as in Fig. 5). The overall error is processed with a PID controller to generate the effective correction. Additionally, a function for the computation of both the input and output shift, i.e. time intervals determining respectively when the received LT data was generated and when the correction will become effective on the robot, is established to further optimize the control performance.

To prevent the excitation of mechanical resonances and ensure safe and effective operation, the generated control action is filtered before entering in the RSI by means of a second order low pass filter. A cutoff frequency of 7 Hz has been set as a trade-off between suppressing unwanted frequencies and maintaining control responsiveness. The robot frequency response has been investigated for many spatial configurations within the previous cubic domain (see Fig. 6) by varying
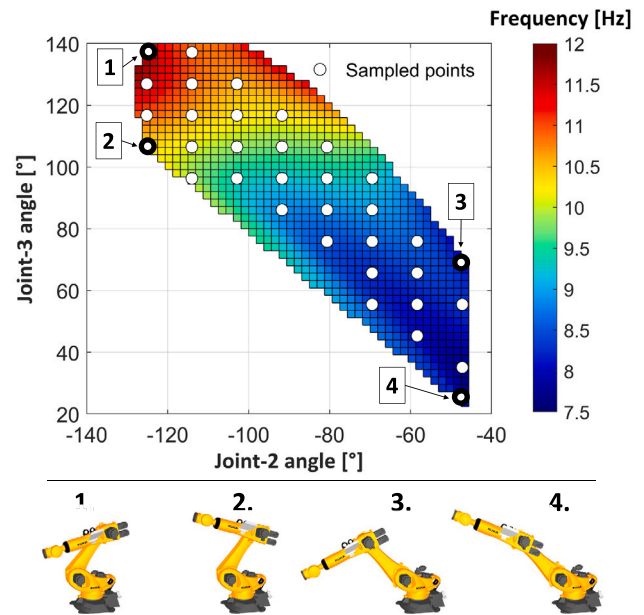

Fig. 17. Map of the robot first natural frequency obtained for *y* movements at different poses within the cubic domain (results fitted with a third-order polynomial surface).

the angular position of joint-2 and joint-3. Following Ref. [42], for each pose, a step motion is commanded along *y* direction (0.5 mm in a single RSI cycle), causing the robot to vibrate. The first natural frequency is then extracted from the LT data. Results have been organized on a two dimensional grid and fitted to yield the empirical surface shown in Fig. 17. Overall, the natural frequency shows high variation on the domain, ranging from the 7.5 to 12 Hz. The imposed filter ensures control stability in the considered workspace. The main drawback is that error contributions at frequencies higher than 7 Hz cannot be compensated. Therefore, on the basis of the results shown in Fig. 15, in the current configuration the online path compensation is expected to be particularly effective for speeds up to 100 mm/s.

To validate the proposed approach, tests have been performed by imposing linear movements along x, *y* or z directions. The control gains have been manually tuned to ensure the best control performance. Alternatively, model-based methods can be adopted to speed up the commissioning phase on large workspaces [43], where the robot dynamic properties are more likely to change, as clearly demonstrated in Fig. 17.

Fig. 18 reports the results obtained for each line, adopting a travel speed of 50 mm/s. In all cases, the robot accuracy has been drastically increased. In particular orthogonal deviation has been reduced of amounts equaling to 93.3%, 80.5% and 64.2%, whereas in-line errors of about 98.4%, 92.8% and 97% respectively for x, *y* and z lines. Overall, the developed compensation module reduces the oscillation amplitude in the frequency range up to 7 Hz, where the main error contributions occurred. Better performance would potentially be achieved by implementing well-tuned band-stop filters which would extend the controller bandwidth.

The proposed approach can be beneficial for various industrial applications that involve precise positioning of tools or components, including assembly, machining, gluing, sealing, painting, coating, and welding. Nevertheless, there are some aspects that need to be considered before implementation, namely: (i) Costs related to LT purchase and maintenance; (ii) Work environment, as the LT measurement is sensitive to temperature, humidity, dust and air flow conditions; (iii) Available space (cell footprint and encumbrances) for installation and resulting measuring distances (as outlined in Section 3.2), which reflects to (iv) LT performance and type/size of measured volume and,
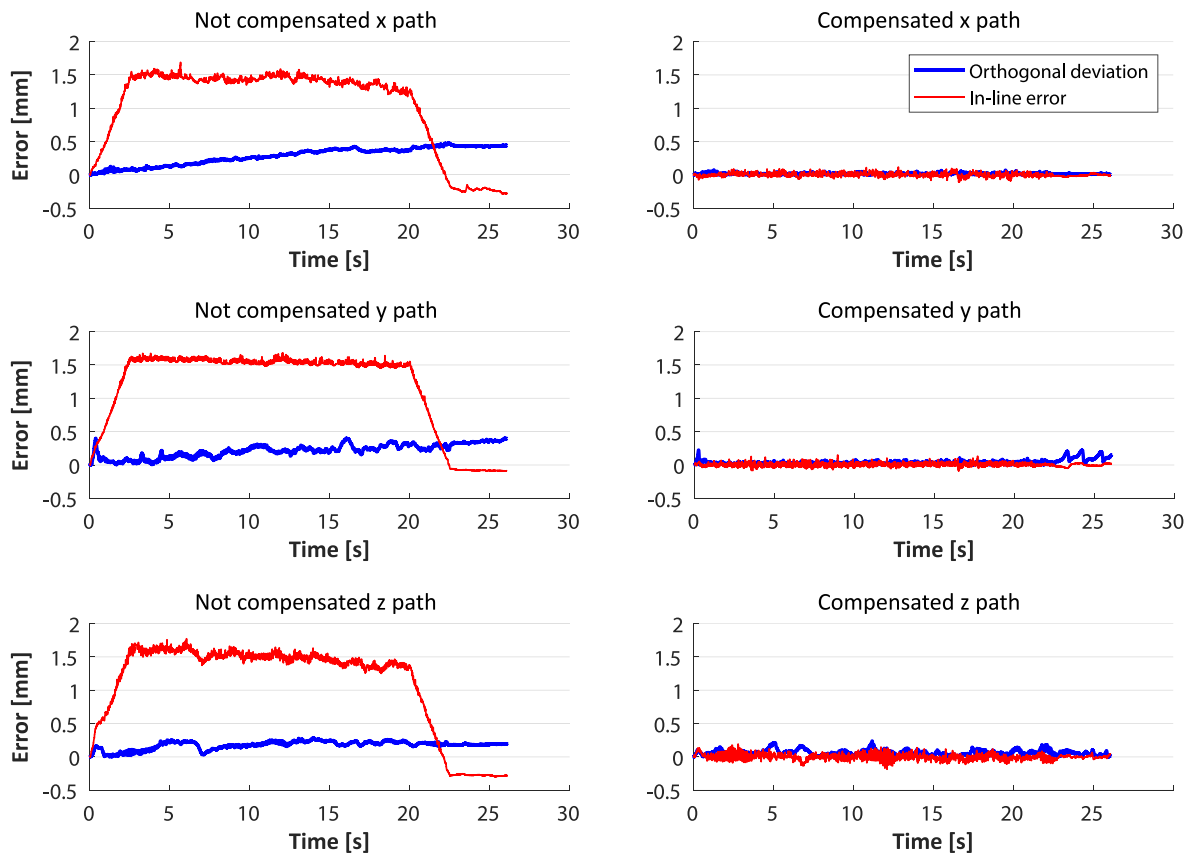
Fig. 18. Comparison between compensated and not compensated paths in x, *y* and z directions.

finally, (v) Time needed for installation and setup (i.e. frame identification, Section 3.3), to be repeated e.g. when the LT is relocated or the SMR is mounted in a different position on the device.

6. Conclusions

The paper reports an engineering method for the evaluation of IR position and path accuracy, which can be applied to any serial manipulator within its working environment. A commercial LT measurement system has been used to develop and validate the proposed procedure in the context of a flexible robotic manufacturing cell, although the method has general validity and can potentially be applied to other measuring systems. The test equipment also comprises a thermal camera for the assessment of the robot thermal state. Following ISO 9283, an experimental campaign is carried out on a KUKA KR210 R2700 Prime robot aimed to provide comprehensive performance maps of the robot pose and path accuracy. Tests are performed for different combinations of robot speeds, payloads and thermal states. During post-processing, statistical tests have been executed to identity and analyze the correlation among input parameters and pose/path accuracy indexes. In the last part of the work, a novel online compensation approach is presented and validated. The cell configuration has been varied to enable real-time robot control through an external controller running on an industrial PC and directly connected to the KUKA RSI module. Despite the need for further improvements aimed at extending the controller bandwidth, the proposed approach yielded remarkable results in reducing orthogonal deviations (by over 64%) and in-line errors (by over 93%), significantly improving the IR path accuracy during the execution of linear movements at a speed of 50 mm/s. This method can be extended to other IR models and used to enhance their usability in high precision applications, such as machining and precise assembly. The experimental data related to this work is made available to the research community for further developments.

Supplementary material

Supplementary material related to this article can be freely downloaded via a Mendeley Data link https://data.mendeley.com/datasets/hpf66pv4nb/1.

Declaration of competing interest

The authors declare that they have no known competing financial interests or personal relationships that could have appeared to influence the work reported in this paper.

Data availability

Data will be made available on request.

Funding sources

References

[1] M. Płaczek, Ł. Piszczek, Testing of an industrial robot's accuracy and repeatability in off and online environment, Eksploat. Niezawodn. 20 (2018) 455–464, http://dx.doi.org/10.17531/ein.2018.3.15.
[2] M. Dehghani, R.A. McKenzie, R.A. Irani, M. Ahmadi, Robot-mounted sensing and local calibration for high-accuracy manufacturing, Robot. Comput.-Integr. Manuf. 79 (2022) http://dx.doi.org/10.1016/j.rcim.2022.102429.
[3] H. Zu, X. Chen, Z. Chen, Z. Wang, X. Zhang, Positioning accuracy improvement method of industrial robot based on laser tracking measurement, in: Measurement: Sensors, Vol. 18, 2021, 100235, http://dx.doi.org/10.1016/j.measen.2021.100235, URL https://www.sciencedirect.com/science/article/pii/S2665917421001987.

[4] C. Lehmann, M. Pellicciari, M. Drust, J.W. Gunnink, Machining with industrial robots: The COMET project approach, in: Communications in Computer and Information Science, Vol. 371, 2013, pp. 27–36, http://dx.doi.org/10.1007/978-3-642-39223-8_3.

[5] C. Moeller, H.C. Schmidt, P. Koch, C. Boehlmann, S. Kothe, J. Wollnack, W. Hintze, Real time pose control of an industrial robotic system for machining of large scale components in aerospace industry using laser tracker system, SAE Int. J. Aerosp. 10 (2017) 100–108, http://dx.doi.org/10.4271/2017-01-2165.

[6] L. Cen, S.N. Melkote, Effect of robot dynamics on the machining forces in robotic milling, in: Procedia Manufacturing, Vol. 10, Elsevier B.V., 2017, pp. 486–496, http://dx.doi.org/10.1016/j.promfg.2017.07.034.

[7] A. Karim, E. Corcione, J.A. Verl, Experimental determination of compliance values for a machining robot, in: IEEE/ASME International Conference on Advanced Intelligent Mechatronics, AIM, Vol. 2018-July, Institute of Electrical and Electronics Engineers Inc., 2018, pp. 1311–1316, http://dx.doi.org/10.1109/AIM.2018.8452434.

[8] D. Sawyer, L. Tinkler, N. Roberts, R. Diver, Improving robotic accuracy through iterative teaching, in: SAE Technical Papers, Vol. 2020-March, SAE International, 2020, p. 7, http://dx.doi.org/10.4271/2020-01-0014.

[9] L. Lattanzi, C. Cristalli, D. Massa, S. Boria, P. Lépine, M. Pellicciari, Geometrical calibration of a 6-axis robotic arm for high accuracy manufacturing task, Int. J. Adv. Manuf. Technol. 111 (2020) 1813–1829, http://dx.doi.org/10.1007/s00170-020-06179-9.

[10] M. Sumanas, A. Petronis, V. Bucinskas, A. Dzedzickis, D. Virzonis, I. Morkvenaite-Vilkonciene, Deep Q-learning in robotics: Improvement of accuracy and repeatability, Sensors 22 (2022) http://dx.doi.org/10.3390/s22103911.

[11] S. Gharaaty, T. Shu, W.F. Xie, A. Joubair, I.A. Bonev, Accuracy enhancement of industrial robots by on-line pose correction, in: 2017 2nd Asia-Pacific Conference on Intelligent Robot Systems, ACIRS 2017, Institute of Electrical and Electronics Engineers Inc., 2017, pp. 214–220, http://dx.doi.org/10.1109/ACIRS.2017.7986096.

[12] D. Patel, L. Lienenlüke, S. Storms, C. Brecher, J. Wied, Improving the absolute accuracy by online interpolation technique of industrial robots, in: IOP Conference Series: Materials Science and Engineering, Vol. 575, Institute of Physics Publishing, 2019, 012013, http://dx.doi.org/10.1088/1757-899X/575/1/012013.

[13] Y. Liu, Y. Li, Z. Zhuang, T. Song, Improvement of robot accuracy with an optical tracking system, Sensors (Switzerland) 20 (2020) 1–26, http://dx.doi.org/10.3390/s20216341.

[14] A.A. Hayat, R.A. Boby, S.K. Saha, A geometric approach for kinematic identification of an industrial robot using a monocular camera, Robot. Comput.-Integr. Manuf. 57 (2019) 329–346, http://dx.doi.org/10.1016/j.rcim.2018.11.008.

[15] A. Nubiola, M. Slamani, I.A. Bonev, A new method for measuring a large set of poses with a single telescoping ballbar, Precis. Eng. 37 (2013) 451–460, http://dx.doi.org/10.1016/j.precisioneng.2012.12.001.

[16] M. Slamani, A. Nubiola, I. Bonev, Assessment of the positioning performance of an industrial robot, Ind. Robot 39 (2012) 57–68, http://dx.doi.org/10.1108/01439911211192501.

[17] Z. Wang, R. Zhang, P. Keogh, Real-time laser tracker compensation of robotic drilling and machining, J. Manuf. Mater. Process. 4 (2020) http://dx.doi.org/10.3390/jmmp4030079.

[18] A. Nubiola, I.A. Bonev, Absolute calibration of an ABB IRB 1600 robot using a laser tracker, Robot. Comput.-Integr. Manuf. 29 (2013) 236–245, http://dx.doi.org/10.1016/j.rcim.2012.06.004.

[19] X. Shi, F. Zhang, X. Qu, B. Liu, An online real-time path compensation system for industrial robots based on laser tracker, Int. J. Adv. Robot. Syst. 13 (2016) 1–14, http://dx.doi.org/10.1177/1729881416663366.

[20] H.N. Nguyen, J. Zhou, H.J. Kang, A new full pose measurement method for robot calibration, Sensors (Basel Switzerland) 13 (2013) 9132–9147, http://dx.doi.org/10.3390/s130709132.

[21] ISO Central Secretary, Manipulating Industrial Robots — Performance Criteria and Related Test Methods, Standard ISO 9283:1998, International Organization for Standardization, 1998.

[22] L. McGarry, J. Butterfield, A. Murphy, Assessment of ISO standardisation to identify an industrial robot's base frame, Robot. Comput.-Integr. Manuf. 74 (2022) http://dx.doi.org/10.1016/j.rcim.2021.102275.

[23] M. Morozov, J. Riise, R. Summan, S.G. Pierce, C. Mineo, C.N. MacLeod, R.H. Brown, Assessing the accuracy of industrial robots through metrology for the enhancement of automated non-destructive testing, in: 2016 IEEE International Conference on Multisensor Fusion and Integration for Intelligent Systems, MFI, 2016, pp. 335–340, http://dx.doi.org/10.1109/MFI.2016.7849510.

[24] J. Santolaria, J. Conte, M. Ginés, Laser tracker-based kinematic parameter calibration of industrial robots by improved CPA method and active retroreflector, Int. J. Adv. Manuf. Technol. 66 (2013) 2087–2106, http://dx.doi.org/10.1007/s00170-012-4484-6.

[25] R.A. Boby, A. Klimchik, Combination of geometric and parametric approaches for kinematic identification of an industrial robot, Robot. Comput.-Integr. Manuf. 71 (2021) http://dx.doi.org/10.1016/j.rcim.2021.102142.

[26] Y. Cho, H.M. Do, J. Cheong, Screw based kinematic calibration method for robot manipulators with joint compliance using circular point analysis, Robot. Comput.-Integr. Manuf. 60 (2019) 63–76, http://dx.doi.org/10.1016/j.rcim.2018.08.001.

[27] J. Santolaria, M. Ginés, Uncertainty estimation in robot kinematic calibration, Robot. Comput.-Integr. Manuf. 29 (2013) 370–384, http://dx.doi.org/10.1016/j.rcim.2012.09.007.

[28] B. Liu, F. Zhang, X. Qu, X. Shi, A rapid coordinate transformation method applied in industrial robot calibration based on characteristic line coincidence, Sensors (Switzerland) 16 (2016) http://dx.doi.org/10.3390/s16020239.

[29] Y.M. Zhao, Y. Lin, F. Xi, S. Guo, Calibration-based iterative learning control for path tracking of industrial robots, IEEE Trans. Ind. Electron. 62 (2015) 2921–2929, http://dx.doi.org/10.1109/TIE.2014.2364800.

[30] M.R. Woodside, J. Fischer, P. Bazzoli, D.A. Bristow, R.G. Landers, A kinematic error controller for real-time kinematic error correction of industrial robots, in: Procedia Manufacturing, Vol. 53, Elsevier B.V., 2021, pp. 705–715, http://dx.doi.org/10.1016/j.promfg.2021.06.069.

[31] T. Kubela, A. Pochyly, V. Singule, High accurate robotic machining based on absolute part measuring and on-line path compensation, in: 2019 International Conference on Electrical Drives Power Electronics (EDPE), 2019 International Conference on Electrical Drives Power Electronics (EDPE), 2019, pp. 143–148.

[32] Z. Wang, P.G. Maropoulos, Real-time laser tracker compensation of a 3-axis positioning system—dynamic accuracy characterization, Int. J. Adv. Manuf. Technol. 84 (2016) 1413–1420, http://dx.doi.org/10.1007/s00170-015-7820-9.

[33] S. Droll, Real time path correction of industrial robots with direct end-effector feedback from a laser tracker, SAE Int. J. Aerosp. 7 (2014) 222–228, http://dx.doi.org/10.4271/2014-01-2248.

[34] M. Gadaleta, G. Berselli, M. Pellicciari, F. Grassia, Extensive experimental investigation for the optimization of the energy consumption of a high payload industrial robot with open research dataset, Robot. Comput.-Integr. Manuf. 68 (2021) http://dx.doi.org/10.1016/j.rcim.2020.102046.

[35] A.L. Reun, K. Subrin, A. Dubois, S. Garnier, Thermal drift and backlash issues for industrial robots positioning performance, Robotica 40 (2022) 2933–2952, http://dx.doi.org/10.1017/S0263574721002022.

[36] K.M. Nasr, A.B. Forbes, B. Hughes, A. Lewis, ASME B89.4.19 standard for laser tracker verification - Experiences and optimisations, Int. J. Metrol. Qual. Eng. 3 (2012) 89–95, http://dx.doi.org/10.1051/ijmqe/2012014.

[37] H. Wang, Z. Shao, Z. Fan, Z. Han, Optimization of laser trackers locations for position measurement, in: I2MTC 2018 - 2018 IEEE International Instrumentation and Measurement Technology Conference: Discovering New Horizons in Instrumentation and Measurement, Proceedings, Institute of Electrical and Electronics Engineers Inc., 2018, pp. 1–6, http://dx.doi.org/10.1109/I2MTC.2018.8409835.

[38] D. Szybicki, P. Obal, K. Kurc, P. Gierlak, Programming of industrial robots using a laser tracker, Sensors 22 (2022) http://dx.doi.org/10.3390/s22176464.

[39] P. Bilancia, L. Monari, R. Raffaeli, M. Peruzzini, M. Pellicciari, Accurate transmission performance evaluation of servo-mechanisms for robots, Robot. Comput.-Integr. Manuf. 78 (2022) http://dx.doi.org/10.1016/j.rcim.2022.102400.

[40] P.K. Sahu, G. Balamurali, B.B. Biswal, Robotic manipulator trajectory optimisation using an improved modified bat algorithm, Int. J. Mechatron. Autom. 7 (1) (2020) 11–22, URL https://www.scopus.com/inward/record.uri?eid=2-s2.0-85089536698&partnerID=40&md5=5eeb853c449894b177445439870ba925.

[41] M. Hollander, D.A. Wolfe, Nonparametric Statistical Methods, John Wiley & Sons, Inc., Hoboken, NJ, 1999.

[42] V. Nguyen, S. Melkote, Hybrid statistical modelling of the frequency response function of industrial robots, Robot. Comput.-Integr. Manuf. 70 (2021) 102134, http://dx.doi.org/10.1016/j.rcim.2021.102134, URL https://www.sciencedirect.com/science/article/pii/S0736584521000193.

[43] T. Cvitanic, S.N. Melkote, A new method for closed-loop stability prediction in industrial robots, Robot. Comput.-Integr. Manuf. 73 (2022) http://dx.doi.org/10.1016/j.rcim.2021.102218.